Dynamics of Excited Hydroxyl Radicals in Hydrogen-Based Mixtures Behind Reflected Shock Waves

R. MÉVEL[a], S. PICHON[b], L. CATOIRE[c], N. CHAUMEIX[b], C.-E. PAILLARD[b] and J.E. SHEPHERD[a]

[a] Graduate Aerospace Laboratories, California Institute of Technology
1200 E. California Blvd, Pasadena, California 91125, USA

[b] Institut de Combustion, Aérothermique, Réactivité et Environnement (ICARE)-CNRS
1C, avenue de la Recherche Scientifique, F - 45071 Orléans Cedex 02, France

[c] Ecole Nationale Supérieure de Techniques Avancées ENSTA-ParisTech
32, boulevard Victor, 75739 Paris Cedex 15, France

Abstract

The chemiluminescence originating from OH*, the excited hydroxyl radical, is one of the most extensively used diagnostics to characterize auto-ignition delay time of gaseous mixtures behind reflected shock waves. We have carried out new experiments and modeling of this diagnostic as well as analyzed previous results for hydrogen-based mixtures, including H_2-O_2, H_2O_2-H_2O, H_2-N_2O and H_2-O_2-N_2O. The experiments were analyzed with a detailed chemical reaction model which included mechanisms for OH* creation, quenching, and emission. Simulations of the reaction behind reflected shock waves were used to predict OH* emission profiles and compare this with measured results as well as profiles of temperature and the ground state concentrations of OH. Analysis of OH* rates of progress demonstrates that a quasi-steady state approximation is applicable and an algebraic model for OH* concentrations can be derived that relates emission to the product of concentrations of O and H for H_2-O_2 and H_2O_2 mixtures and an additional contribution by the product of H and N_2O when N_2O is an oxidizer.

Keywords :

Excited hydroxyl radical; Reflected shock wave, Hydrogen, High temperature chemical kinetics

Introduction

Over the past 60 years, the shock-tube technique has been extensively used in high temperature chemical kinetics [1], notably for the determination of fundamental parameters such as auto-ignition delay-time [1,2]. Auto-ignition delay-time is a very important parameter to characterize the high-temperature behaviour of fuel-oxidant mixtures with applications to propulsion, car engine and industrial safety, among others [1]. A widely-used diagnostic to measure delay-times behind reflected shock wave is based on the chemiluminescence near 306 nm, corresponding to the ($A^2\Sigma^+$-$X^2\Pi$) transition of excited OH radicals, OH* [2-4]. A number of studies [4-10] have been performed to determine the rate constants of the reactions producing and consuming OH*. Ibraguimova et al. [11] and Smekhov et al. [12] reviewed the rate constants involving excited species in hydrogen-oxygen mixtures. The OH* reaction mechanism includes formation processes, the most significant of which is considered to be H+O+M=OH*+M, collision quenching with other species, and one radiative de-excitation process with a decay time of 0.7 μs. The excitation of OH radical through vibrational energy transfer during collisions is usually neglected. Because OH* is present in very low concentrations and does not play a significant role in combustion chemistry, it is omitted from most detailed reaction models [13-17] Recently, Hall et al. [2] systematically compared experimental OH* emission features (or profiles) and characteristic ignition times with simulation results involving both the ground-state and the excited OH radicals. They concluded that for many hydrocarbon-oxygen-argon mixtures, a sub-mechanism describing OH* chemistry should be included for greater consistency when modeling OH* based experimental data.

The purposes of the present study are to extend the study of Hall to other oxidizers and hydrogen-based mixtures including H_2-O_2-Ar, H_2O_2-H_2O-Ar and H_2-N_2O(-O_2)-Ar mixtures. We have carried out shock tube experiments and modeling of OH* emission with chemical

reaction models appropriate for these mixtures. The results were first compared to the existing data and model results on the H_2-O_2-Ar system before examining mixtures with H_2O_2 and N_2O.

Materials and Methods

Mixtures preparation

All gases were of research grade (Air Liquide). A hydrogen peroxide-water solution (70% H_2O_2–30% H_2O by mass) was used to prepare the H_2O_2-H_2O-Ar mixtures. The partial pressure method was used to prepare the mixtures in a stainless-steel vessel or in a glass vessel for H_2O_2 based mixtures. Homogeneity of the mixtures was obtained by active mixing for several hours. The mixture compositions and the experimental conditions are summarized in Table 1.

Experimental apparatus

Two shock-tubes were employed to perform the experiments. A glass shock-tube (Orléans) was used for the H_2O_2-H_2O-Ar mixtures, to prevent adsorption and premature decomposition of H_2O_2. This tube (i.d. 50mm) has a 2m long driver section and a test section about 9m long. The second shock-tube (Caltech) is composed of three parts separated by two diaphragms and is made of stainless steel. The driver section and the driven section are 6.19 and 11.28m long, respectively, (i.d. 15.24cm). The test section is 2.44m long (i.d. 7.62cm). A 2.03m long (i.d. 7.62cm) cookie-cutter is used to transmit the shock wave from the driven to the test section, avoiding perturbation of the incident shock wave. The driver gas was helium. The test sections of the two shock-tubes were equipped with several diagnostic instruments located close to the end wall: four piezoelectric pressure transducers, mounted flush with the inside wall, for shock velocity measurements (uncertainty below 2%), and a calcium fluoride or quartz optical window mounted at 10 mm from the tube end, associated with, a narrow slit or

an optical fiber, a 306 nm band-pass filter and a photomultiplier. Depending on the mixture, different definitions were employed for the auto-ignition delay-time. These were τ_{onset} for the onset of emission (intersection of the tangent to (dOH*/dt)max with the zero emission line), and $\tau_{50\%}$ and $\tau_{100\%}$ for the time to reach 50% and 100% of the OH emission peak, respectively. Table 1 gives the definition used for each mixture studied. Uncertainty for the delay-time is on the order of 20% except for H_2O_2-H_2O-Ar for which it is around 30% because of the very low signal intensity.

Chemical kinetic scheme

The detailed reaction model presently used is that of Mével et al. [3,18]. The sub-mechanism for OH* radical chemistry was taken from Hall et al. [2,4,5] and Hidaka et al. [6,7] studies. A few modifications were made concerning H_2O_2 related chemistry as described in Pichon [19]. Briefly, the rate constants of the reactions $H_2O_2+OH=HO_2+H_2O$, $HO_2+OH=H_2O+O_2$, $HO_2+HO_2=H_2O_2+O_2$, were adjusted within the uncertainty limits given by Kappel et al. [20]. Also, the $H_2O_2(+M)=2OH(+M)$ decomposition reaction was replaced by individual reactions with specific rate constants for each of the following collision partners: H_2, H_2O_2, Ar and H_2O. These rate constants were taken from [21-23]. The reaction model (see supplemental material) was validated with respect to a wide range of experimental data including shock-tube data for H_2-O_2 and H_2-N_2O mixtures [24].The modeling of the experimental results was performed with SENKIN [25] using the constant volume reactor model. Sensitivity, rate of production and energy release rate analyses were performed using this code. The energy release rates per reaction, corresponding to the reaction enthalpy multiplied by the net reaction rate, are referred to as “energy profiles” in the figures.

Results and discussion

Experimental results for H_2-O_2-Ar, H_2O_2-H_2O-Ar and H_2-N_2O(-O_2)-Ar mixtures are presented along with the model predictions for each type of mixture Comparisons are given for five additional reaction models in the supplemental material.

Hydrogen-oxygen mixtures

Figures 1 and 2 compare the time to emission onset of several H_2-O_2-Ar mixtures obtained experimentally and the onset times obtained from calculated OH* or OH concentration profiles. Both the data from the present study (Fig. 1) and data from Petersen et al. [26] (Fig. 2) demonstrate the consistency between the experimental emission onset and calculated concentration onset times for either species.

Figure 3 compares the experimental emission profile and the calculated OH* and OH concentration profiles as well as the rates of production, ROP, profiles for those two species in Mixture 2. Unlike what was found by Hall et al. for hydrocarbon-oxygen mixtures [2], the emission profile is matched very well up to its maximum by both OH* and OH radical profiles. However, the decay period is much better reproduced by the OH* profile. This is due to the very fast quenching of the excited radical compared to the slower consumption of the ground-state radical. The production of OH* is only due to H+O+M=OH*+M whereas the OH formation is driven by the two O+H_2=OH+H and H+O_2=OH+O branching reactions. Because the precursors of OH* and OH radicals are the same, H and O for instance, their respective temporal profiles are strongly correlated with each other. The lower probability of the trimolecular process forming OH* compared to the branching process forming OH, accounts for the ratio $X_{OH}/X_{OH^*}=10^6$. From this reaction pathway analysis, the dynamics of OH* in H_2-O_2 mixtures can be described by the following reduced scheme:

R1: H+O+M=OH*+M

R2: OH*+M=>OH+M

R3: OH*=>OH+hν

Applying the quasi-steady-state-approximation (QSSA) to OH* leads to

$$[OH^*]_{Steady\_State} = \frac{k_1[O][H][M]}{(k_2 + k_{-1})[M] + k_3}$$

Comparisons between the $[OH^*]_{Full\_Model}$ and $[OH^*]_{Steady\_State}$ demonstrate very good agreement as seen in the supplemental material (Fig S5). This indicates that in the present experiments, OH* emission temporal dependence is primarily a function of the H and O concentration time dependence and OH* quenching processes serve to primarily determine the peak amplitude of emission. The influence of ground state OH arises through the coupling to the chain branching processes that couple the O, H and OH concentrations.

Figure 4 shows the temperature and temperature gradient profiles as well as the rates of energy production per reaction. The time at which the emission peaks, around 100 μs, corresponds closely to the time to the maximum of the temperature gradient profile. The main reaction responsible for energy release is $OH+H_2=H_2O+H$ whereas the hydroperoxide radical decomposition reaction is the main reaction absorbing energy.

Hydrogen peroxide-water vapour mixtures

The experimental $\tau_{50\%}$ and $\tau_{100\%}$ times (Fig. 5 and 6) and the times derived from the computed OH* profiles have a mean difference of 38% which is on the same order as the experimental uncertainty, 30%. The times are usually underestimated (by 15 μs on average), especially for mixture 7 with an argon dilution of 99.5%. The effective activation energy observed experimentally is reproduced within 20% by the model. Contrary to observations on H_2-O_2-Ar mixtures, the profile of the ground-state OH radicals is uncorrelated with that of OH* and OH delay-times as much as two orders of magnitude smaller than those of OH*.

Figure 7 displays the experimental emission profile and the calculated OH* and OH profiles as well as the ROP profiles for those two species. As previously mentioned, the emission intensity was very low for the H_2O_2-H_2O-Ar mixtures, which explains the low signal-to-noise

ratio. The calculated OH* concentrations are typically at least 100 times lower than in an equivalent H_2-O_2-Ar mixture. The calculated OH* concentration profile is in reasonable agreement with the experimental emission profile up to 150 μs. The ground state OH reaches a peak much earlier and it decays much faster than OH*. As in the H_2-O_2-Ar mixtures, excited OH radicals are formed by the H+O+M=OH*+M reaction. They are mainly consumed through collisional quenching by water.

The respective time scales of OH and OH* radicals are very different (Figure 7) and contrary to what is observed for the H_2-O_2-Ar mixtures, the OH appears first and rapidly decays, followed by the appearance of OH* which decays much more slowly. This is because OH is the direct decomposition product of H_2O_2 and not until OH is consumed by reactions with HO_2 and H_2O_2 are H, O, and OH* then formed later in time. In this system, it is therefore essential to include a sub-mechanism describing OH* chemistry to properly utilize OH* emission profile as a diagnostic. Calculations performed for H_2-H_2O_2-H_2O-Ar cases indicate that this is also the case in that mixture (See supplemental material Figures S1 and S2). The QSSA analysis given above for H_2-O_2 mixtures also applies to H_2O_2 mixtures (see supplemental material Fig S6).

Figure 8 presents the temperature and temperature gradient profiles along with the rates of energy production per reaction. Although the initial conditions were the same as those displayed in Figure 7, the range of the time scale was reduced to 20 μs. The time to the peak of the temperature gradient profile agrees with the time to the OH radical peak. Unlike the H_2-O_2-Ar mixtures, the OH* emission profile is not well correlated with the energy release profile. After an initial period of temperature drop due to the endothermic decomposition of H_2O_2, energy is released by the two HO_2+OH=H_2O+O_2 and H_2O_2+OH=H_2O+HO_2 reactions.

Hydrogen-nitrous oxide(-oxygen) mixtures

The experimental $\tau_{50\%}$ times of H_2-N_2O-Ar and H_2-N_2O-O_2-Ar mixtures are compared in Fig. 9 to delay times calculated from OH* and OH concentration profiles. Data from the present tests as well as from the literature [3,27] are considered. For hydrogen-nitrous oxide mixtures, the predictions of the reaction model are relatively satisfactory using OH* profiles and the average error is 22%. The ground-state OH concentration significantly (up to 78% in $\tau_{50\%}$) lags the OH* concentration. For H_2-O_2-N_2O-Ar mixtures, the OH* emission delay-times are slightly underestimated; the mean error in the prediction is 17% using the computed OH* profiles. The OH and OH* profiles are well correlated for H_2-O_2-N_2O-Ar mixtures

The delay-times for H_2-O_2-N_2O-Ar mixtures are much shorter, up to 4 times than those measured for H_2-N_2O-Ar mixtures, in the lower temperature range and the effective activation energy is almost two times lower. The ignition process in H_2-N_2O-Ar mixtures essentially proceeds through a linear sequence: $N_2O(+M)=N_2+O(+M)$; $O+H_2=OH+H$; $N_2O+H=N_2+OH$; $OH+H_2=H_2O+H$. The reaction runaway is driven by the very exothermic $N_2O+H=N_2+OH$ reaction. In H_2-O_2-N_2O-Ar mixtures, in addition to this linear process, the classical $O+H_2=OH+H$ and $H+O_2=OH+O$ branching process occurs, which increases the overall reaction rate and decreases the reaction time.

Figure 10 shows the experimental emission profile and the calculated OH* and OH profiles as well as the ROP profiles for those two species. The emission profile is in good agreement with the calculated OH* profile up to 100 μs and the decay rate is also reasonably well matched. The onsets of OH and OH* are temporally coherent since both species originate from the reaction between N_2O and H. However, OH radicals are immediately consumed by reacting with H_2 so that their relative production rate is slower than that of OH*. In H_2-O_2-N_2O-Ar mixtures (See supplemental material Figure S3), the $N_2O+H=N_2+OH^*$ reaction does not contribute significantly to OH* production. The primary path for OH formation is $N_2O+H=N_2+OH$. However, unlike the H_2-N_2O-Ar mixtures, the consumption of OH by

reaction with H_2 is counterbalanced by the branching process, so that OH* and OH profiles appear coherent in time as in H_2-O_2-Ar mixtures. In order to perform a QSSA for these mixtures, the reaction R4: $N_2O+H=N_2+OH^*$ has to be included in the reduced scheme. The expression for [OH*] thus becomes

$$[OH^*]_{Steady\_State} = \frac{k_1[O][H][M] + k_4[N_2O][H]}{(k_2 + k_{-1})[M] + k_{-4}[N_2] + k_3}$$

Comparisons between the $[OH^*]_{Full\_Model}$ and $[OH^*]_{Steady\_State}$ demonstrate very good agreement as seen in the supplemental material (Fig S7 and S8).

Figure 11 presents the temperature and temperature temporal gradient profiles as well as the rates of energy production per reaction. The time at which the emission peaks, around 130 μs, corresponds closely to the time at which the temperature temporal gradient peaks. No simple relationship exists between the OH radical and temperature profiles. The main reaction responsible for energy release is $N_2O+H=N_2+OH$. This reaction is also the most important in the case of H_2-O_2-N_2O-Ar mixtures (See supplemental material Figure S4). For these mixtures, the time to emission maximum corresponds to the time of maximum energy release.

Conclusion

In the present study, hydrogen-based mixtures, including H_2-O_2, H_2O_2-H_2O, H_2-N_2O and H_2-O_2-N_2O, have been studied experimentally using the shock tubes and modeling with detailed chemical reaction mechanisms. The present results, along with those previously obtained by Katthrotia [10] Hall et al. [2] and for various hydrocarbon-oxygen mixtures, demonstrates the need for reliable sub-mechanisms describing OH* radical chemistry in order to properly interpret emission profiles, particularly with oxidizers such as nitrous oxide or hydrogen peroxide. The relationship between the OH* emission and the temperature profile depends on the mixture studied so that OH* emission is not always a good surrogate for energy release rate. We have carried out an analysis of the production and destruction rates of OH* and

found that under our conditions, we can perform a quasi-steady-state-approximation to determine the OH* concentration. This analysis demonstrates that under our experimental conditions OH* is proportional to the [H][O] product for H_2-O_2 and H_2O_2 mixtures, and there is an additional additive dependence on [H] when N_2O is the only oxidant. The role of quenching is to determine the amplitude of the emission signal but not the temporal dependence under the highly-dilute, nearly isothermal conditions that we are considering.

Acknowledgements

The authors acknowledge Aurélien Demenay, Université d'Orléans, and Jason Damazo, Caltech, for their help in setting-up the shock-tube at the Explosion Dynamics Laboratory at Caltech.

References

1. **K. Bhaskaran and P. Roth**, Prog. Energy Combust. Sci. 28 (2002) 151-192.

2. **J.M. Hall, M.J.A. Rickard and E.L. Petersen**, Combust. Sci. and Tech. 177 (2005), 455-483.

3. **R. Mével, S. Javoy, F. Lafosse, N. Chaumeix, G. Dupré, C.-E. Paillard**, Proc. Combust. Instit. 32 (2009) 359-366.

4. **J.M. Hall and E.L. Petersen**, Int. J. Chem. Kinet. 38 (2006) 714-724.

5. **J.M. Hall and E.L. Petersen**, AIAA Paper No 2004-4164, 2004.

6. **Y. Hidaka, H. Takuma and M. Suga**, J. phy. chem. 89 (1985) 4903-4905.

7. **Y. Hidaka, S. Takahashi, H. Kawano and M. Suga**, J. phy. chem. 86 (1982) 1429-1433.

8. **P. Paul, J. Durant, J. Gray, and M. Furlanetto**, J. chem.. phy. 102 (1995) 8378-8384.

9. **M. Tamura, P. Berg, J. Harrington, J. Luque, J. Jeffries, G. Smith D. Crosley**, Combust. Flame 114 (1998) 502-514.

10. **T. Kathrotia, M. Fikri, M. Bozkurt, M. Hartmann, U. Riedel, C. Schulz**, Combust. Flame 157 (2010) 1261-1273.

11. **L.V. Ibraguimova, G.D. Smekhov and O.R. Shatalov**, Recommended rate constants of chemical reactions in H_2–O_2 gas mixture with electronically excited species $O_2(1\Delta)$, $O(1D)$, $OH(2\Sigma)$ involved, Report, Institute of Mechanics of Lomonosov Moscow State Unversity, 2003.

12. **G.D. Smekhov, L.B. Ibraguimova, S. P. Karkach, O.V. Skrebkov and O.P. Shatalov**, High temperature 45 (2007) 395-407.

13. **A.A. Konnov**, Combust. Flame 156 (2009) 2093-2105.

14. **H. Wang, Y. Xiaoqing, V.J. Ameya, G.D. Davis, A. Laskin, F. Egolfopoulos and C.K. Law**, USC Mech Version II. High-temperature combustion reaction model of H_2/CO/C_1-C_4 compounds. Available at: http://ignis.usc.edu/USC_Mech_II.htm, 2007.

15. **B. Sirjean, E. Dames, D. A. Sheen, X.-Q. You, C. Sung, A. T. Holley, F. N. Egolfopoulos, H. Wang, S. S. Vasu, D. F. Davidson, R. K. Hanson, H. Pitsch, C. T. Bowman, A. Kelley, C. K. Law, W. Tsang, N. P. Cernansky, D. L. Miller, A. Violi, R. P. Lindstedt**, A high-temperature chemical kinetic model of *n*-alkane oxidation, JetSurF version 0.2, Available at: http://melchior.usc.edu/JetSurF/Version0_2/Index.html, 2008.

16. **G. P. Smith, D.M. Golden, M. Frenklach, N.W. Moriarty, B. Eiteneer, M. Goldenberg, C.T. Bowman, R.K. Hanson, S. Song, W.C. Gardiner Jr., V.V. Lissianski, and Z. Qin**, GRI-mech release 3.0, Available at: http://www.me.berkeley.edu/gri-mech/.

17. **Z. Hong, D.F. Davidson and R.K. Hanson**, Combust. Flame 158 (2011) 633-644.

18. **R. Mével, S. Javoy and G. Dupré**, Proc. Combust. Instit. 33 (2011) 485–492.

19. **S. Pichon**, Etude cinétique de systems hypergoliques et propergoliques à base d'éthanol et de péroxyde d'hydrogène, PhD thesis, University of Orléans, Orléans, France, 2005.

20. **C. Kappel, K. Luther and J. Troe**, Phys. Chem. Chem. Phys. 4 (2002) 4392-4398.

21. **O. V. Skrebkov, Yu. P. Myagkov, S. P. Karkach et al.**, Doklady Akademii Nauk 383 (2002) 782-785.

22. **D.L. Baulch, C.J. Cobos, R.A. Cox et al.**, J. Phys Chem Ref Data, 23 (1994) 847-1033.

23. **NIST**, National Institute of Standards and Technology, Chemical Kinetics Database, Available at: http://kinetics.nist.gov/kinetics/index.jsp.

24. **R. Mével**, Etude de mécanismes cinétiques et des propriétés explosives des mélanges hydrogène-protoxyde d'azote et silane-protoxyde d'azote. Application à la sécurité industrielle, PhD thesis, University of Orléans, Orléans, France, 2005.

25. **A.E. Lutz, R.J. Kee, A.J. Miller**, SENKIN : a fortran program for predicting homogeneous gas phase chemical kinetics with sensitivity analysis, Report No Sand87-8248, Sandia International Laboratories, 1992.

26. **Petersen E.L., Kalitan D.M. and Rickard M.J.A.**, J Prop Power 20 (2004) 665-674.

27. **Mével R., Lafosse F., Catoire L., Chaumeix N., Dupré G. and Paillard C.E.**, Combust. Sci. and Tech. 180 (2008) 1858-1875.

Figure Captions

Figure 1:

Experimental and calculated τ_{onset} for H_2-O_2-Ar mixtures. Solid lines: delay derived from OH*, Dashed lines: delay derived from OH.

Figure 2:

Experimental and calculated τ_{onset} for H_2-O_2-Ar mixtures. Data from Petersen et al. [26]. Solid lines: delay derived from OH*, Dashed lines: delay derived from OH.

Figure 3:

Rates of production, ROP, for OH* and OH (top) and experimental emission and calculated OH* and OH profiles (bottom) for H_2-O_2-Ar mixtures. Solid lines: ROP for OH*, Dashed lines: ROP for OH.

Figure 4:

Calculated temperature and temperature gradient profile (top) and normalized energy release rates per reaction (bottom) for H_2-O_2-Ar mixtures.

Figure 5:

Experimental and calculated $\tau_{50\%}$ and $\tau_{100\%}$ for a H_2O_2-H_2O-Ar mixture. Solid lines: delay derived from OH*, Dashed lines: delay derived from OH.

Figure 6:

Experimental and calculated $\tau_{50\%}$ and $\tau_{100\%}$ for a H_2O_2-H_2O-Ar mixture. Solid lines: delay derived from OH*, Dashed lines: delay derived from OH.

Figure 7:

Rates of production, ROP, for OH* and OH (top) and experimental emission and calculated OH* and OH profiles (bottom) for a H_2O_2-H_2O-Ar mixture. Solid lines: ROP for OH*, Dashed lines: ROP for OH.

Figure 8:

Calculated temperature and temperature gradient profile (top) and normalized energy release rates per reaction (bottom) for a H_2O_2-H_2O-Ar mixture.

Figure 9:

Experimental and calculated $\tau_{50\%}$ for H_2-N_2O-(O_2)-Ar mixtures. Solid lines: delay derived from OH*, Dashed lines: delay derived from OH.

Figure 10:

Rates of production, ROP, for OH* and OH (top) and experimental emission and calculated OH* and OH profiles (bottom) for a H_2-N_2O-Ar mixture. Solid lines: ROP for OH*, Dashed lines: ROP for OH.

Figure 11:

Calculated temperature and temperature gradient profile (top) and normalized energy release rates per reaction (bottom) for a H_2-N_2O-Ar mixture.

Figures

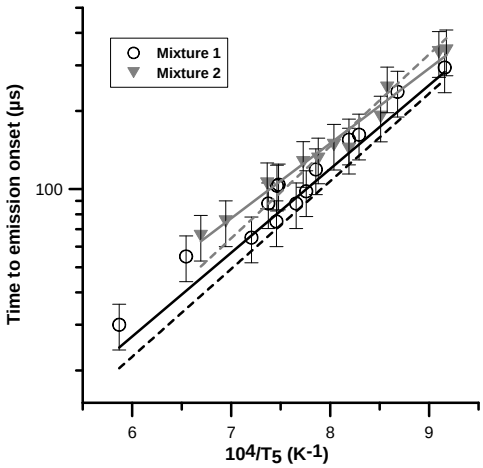

Figure 1: Experimental and calculated τ_{onset} for H_2-O_2-Ar mixtures. Solid lines: delay derived from OH*, Dashed lines: delay derived from OH.

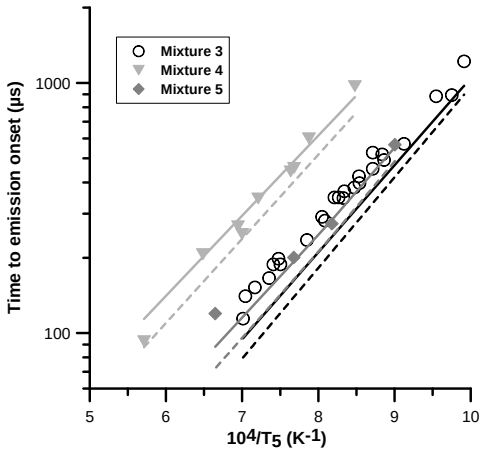

Figure 2: Experimental and calculated τ_{onset} for H_2-O_2-Ar mixtures. Data from Petersen et al. [26]. Solid lines: delay derived from OH*, Dashed lines: delay derived from OH.

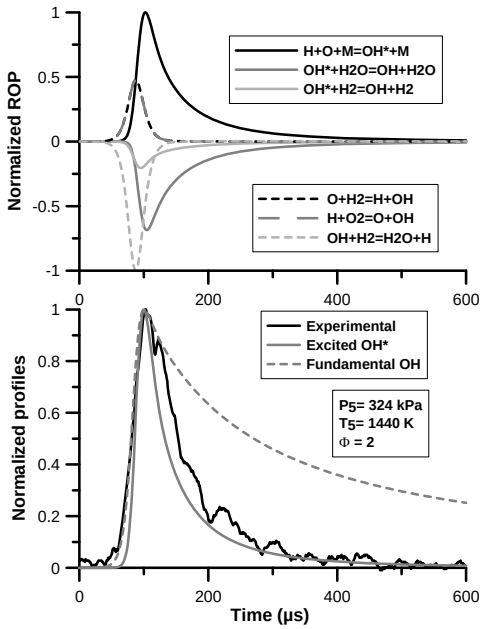

Figure 3: Rates of production, ROP, for OH* and OH (top) and experimental emission and calculated OH* and OH profiles (bottom) for H_2-O_2-Ar mixtures. Solid lines: ROP for OH*, Dashed lines: ROP for OH.

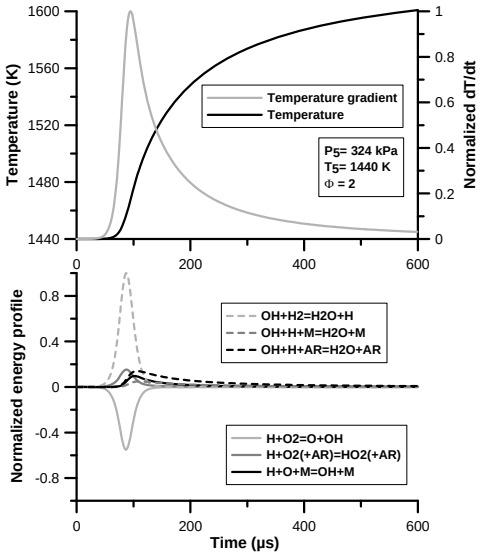

Figure 4: Calculated temperature and temperature gradient profile (top) and normalized energy release rates per reaction (bottom) for H_2-O_2-Ar mixtures.

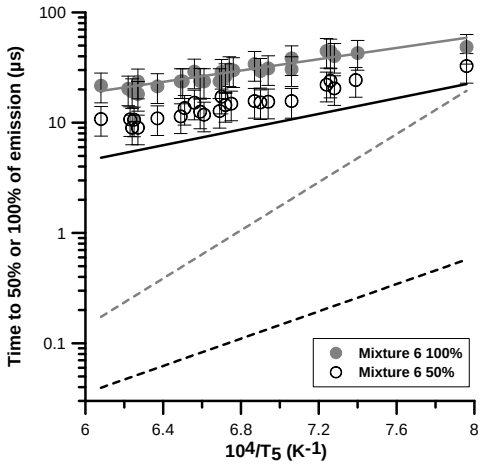

Figure 5: Experimental and calculated $\tau_{50\%}$ and $\tau_{100\%}$ for a H_2O_2-H_2O-Ar mixture. Solid lines: delay derived from OH*, Dashed lines: delay derived from OH.

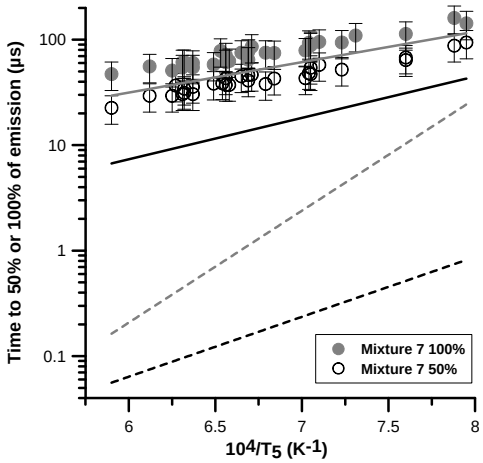

Figure 6: Experimental and calculated $\tau_{50\%}$ and $\tau_{100\%}$ for a H_2O_2-H_2O-Ar mixture. Solid lines: delay derived from OH*, Dashed lines: delay derived from OH.

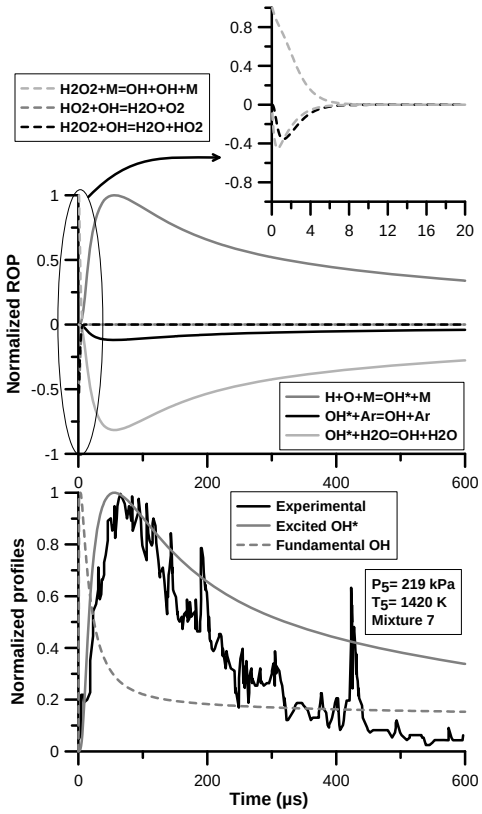

Figure 7: Rates of production, ROP, for OH* and OH (top) and experimental emission and calculated OH* and OH profiles (bottom) for a H_2O_2-H_2O-Ar mixture. Solid lines: ROP for OH*, Dashed lines: ROP for OH.

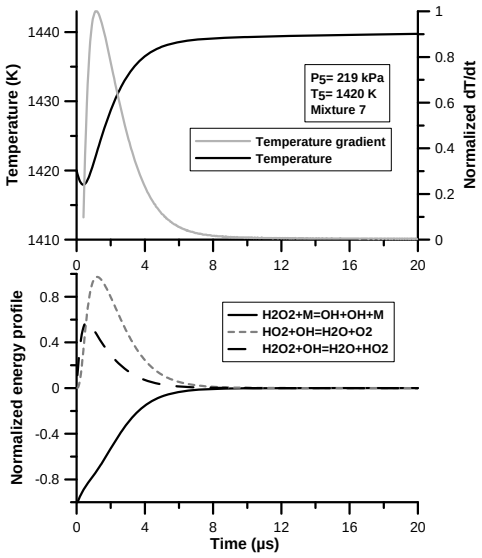

Figure 8: Calculated temperature and temperature gradient profile (top) and normalized energy release rates per reaction (bottom) for a H_2O_2-H_2O-Ar mixture.

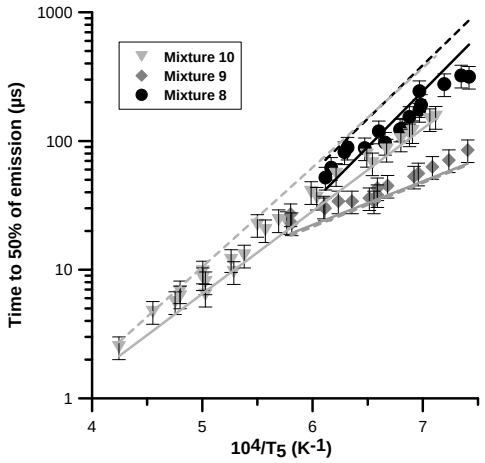

Figure 9: Experimental and calculated $\tau_{50\%}$ for H_2-N_2O-(O_2)-Ar mixtures. Solid lines: delay derived from OH*, Dashed lines: delay derived from OH.

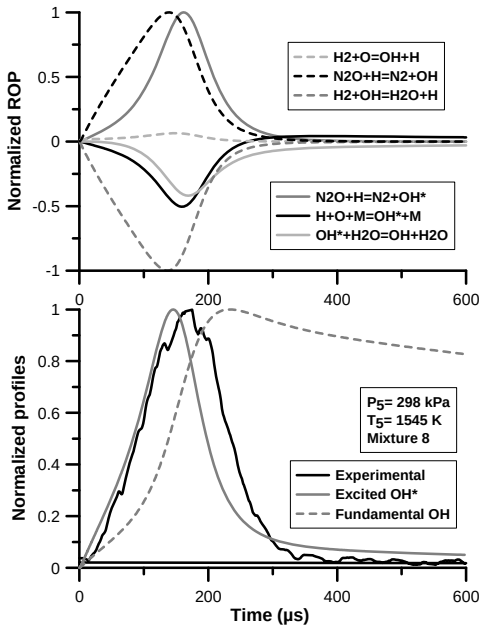

Figure 10: Rates of production, ROP, for OH* and OH (top) and experimental emission and calculated OH* and OH profiles (bottom) for a H_2-N_2O-Ar mixture. Solid lines: ROP for OH*, Dashed lines: ROP for OH.

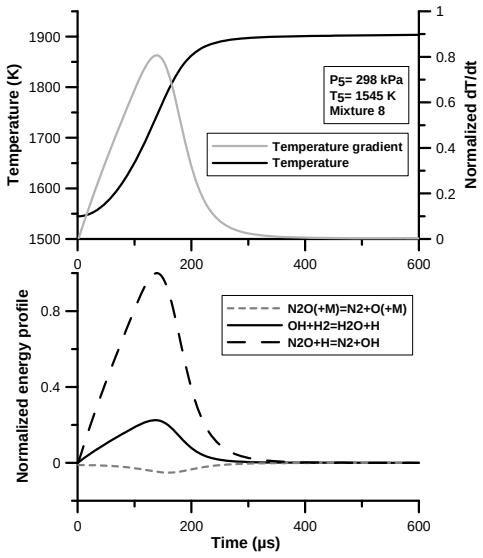

Figure 11: Calculated temperature and temperature gradient profile (top) and normalized energy release rates per reaction (bottom) for a H_2-N_2O-Ar mixture.

Table Captions

Table 1:

Mixture compositions and experimental conditions examined in the present study. In all cases, the diluent is Argon.

Table

Table 1: Mixture compositions and experimental conditions examined in the present study. In all cases, the diluent is Argon.

N°	Φ	X_{H2}	X_{O2}	X_{N2O}	X_{H2O2}	X_{H2O}	T_5 (K)	P_5 (kPa)	Parameter	Ref
1	1.04	0.0169	0.0081	-	-	-	1092-1704	285-410	τ_{onset}	This study
2	2.00	0.0200	0.0050	-	-	-	1090-1494	320-411	τ_{onset}	This study
3	1.00	0.0300	0.0150	-	-	-	1009-1426	101	τ_{onset}	[26]
4	1.03	0.0103	0.0050	-	-	-	1171-1750	101	τ_{onset}	[26]
5	1.47	0.0336	0.0114	-	-	-	1111-1505	101	τ_{onset}	[26]
6	-	-	-	-	0.0055270	0.0044730	1260-1650	150-230	$\tau_{50\%}$ and $\tau_{100\%}$	This study
7	-	-	-	-	0.0027635	0.0022365	1260-1700	170-230	$\tau_{50\%}$ and $\tau_{100\%}$	This study
8	0.97	0.0153	-	0.0158	-	-	1348-1635	282-359	$\tau_{50\%}$	This study
9	0.68	0.0160	0.0076	0.0084	-	-	1350-1724	288-371	$\tau_{50\%}$	This study
10	0.50	0.0033	-	0.0067	-	-	1405-2356	256-320	$\tau_{50\%}$	[3]